Presented at ISABE 2019: 24th Conference of the International Society of Air Breathing Engines, 22-27 September 2019 Canberra, Australia, Paper no. 24197

https://isabe.org/

Low-order models for the calculation of compressor sub-idle characteristics

Mauro Righi, Luis E. Ferrer-Vidal, Alessandro Allegretti, Vassilios Pachidis
m.righi@cranfield.ac.uk
Cranfield University
Centre for Propulsion Engineering
Cranfield
United Kingdom

Richard J. Tunstall
Rolls Royce plc.
Filton, Bristol
United Kingdom

ABSTRACT

This paper focuses on the development of low-order models for the generation of compressor sub-idle characteristics via numerical simulation of an axial-flow compressor at sub-idle conditions. A through-flow code using body forces developed by Cranfield University is used as a framework to test three new methods to model blade row performance under sub-idle conditions. The first method is a simplified analytical model of a separated blade passage, originally developed to model reverse flow through the passage. The method consists of a modification to the body forces employed by the code and can be easily adapted to model the sub-idle operating condition. The second method is a set of pressure loss and deviation angle correlations developed at Cranfield University specifically for sub-idle conditions. A third approach makes use of the deviation angle correlations along with the modified body-force method, resulting in a hybrid approach. These three methods are implemented in the through-flow code to obtain low-order models that are then used to generate compressor characteristics under locked rotor and windmilling conditions. The code created is able to generate compressor characteristics throughout the sub-idle operating regime in a few minutes. The low-order model results are compared against experimental data from a sub-idle compressor rig and CFD RANS simulations of the same compressor. The generated characteristics show promising results, with only minor calibration required for the numerically calculated characteristics to match those generated via experiment.

Keywords: Axial Compressors, Sub-idle conditions, Performance, Simulation and Design

NOMENCLATURE

HPC	High pressure compressor
LES	Large eddy simulation
PS, SS	Pressure side, suction side
RANS	Reynolds-averaged Navier-Stokes
SBES	Stress blended eddy simulation
TVD	Total variation diminishing

Symbols

b	Longley's blockage parameter $[-]$
E_0, H_0	Internal energy, Enthalpy $[\,J/m^3]$
f	Volumetric force $[\,N/m^3]$
h	Grid size $[m]$
I	Shaft inertia $[kg\ \cdot\ m^2]$
i	Incidence angle $[deg]$
W_{EX}	Work exchange $[\,W/m^3]$
M	Mach number $[-]$
$\dot{m}'$	Design point normalised corrected mass-flow $[-]$
P	Pressure $[Pa]$
r	Radius $[m]$
Re	Reynolds number $[-]$
T	Temperature $[T]$
T, dt	Time, time step $[s]$
U	Blade velocity $[m/s]$
u	Flow velocity $[m/s]$
x	Axial position $[m]$
X	Generic variable $[-]$
α	Air flow angle $[rad]$
β	Camber-line direction $[rad]$
γ	Stagger angle $[rad]$
δ	Deviation angle $[rad]$
θ	Circumferential position $[rad]$
ρ	Density $[\,kg/m^3]$
σ	Solidity $[-]$
τ, τ_P	Torque $[N \cdot m]$, Corrected torque parameter $[N \cdot m/Pa]$
Ω, Ω'	Rotational speed $[rad/s]$, Normalised rotational speed $[-]$
ω	Pressure loss coefficient $[-]$

Subscripts

r, x, θ	Radial, axial, circumferential direction
IN	Blade row inlet conditions
$FINE$	Property of the fine grid

1.0 INTRODUCTION

An aviation engine is exposed to the sub-idle regime on start-up or during windmill relight. While these events have historically not warranted a detailed performance evaluation, more stringent certification standards, customer requirements and the push for marginal benefits in fuel efficiency have highlighted the need for accurate sub-idle performance characterization [1]. Additionally, modern engines with increasing by-pass ratios put a strain on relight capability, while larger gearboxes and driven accessories also contribute to increased windmilling drag and reduced starting performance [2]. As the trend for higher by-pass ratios and geared configurations continues to increase, so

too does the need for improved sub-idle performance, requiring improved prediction techniques.

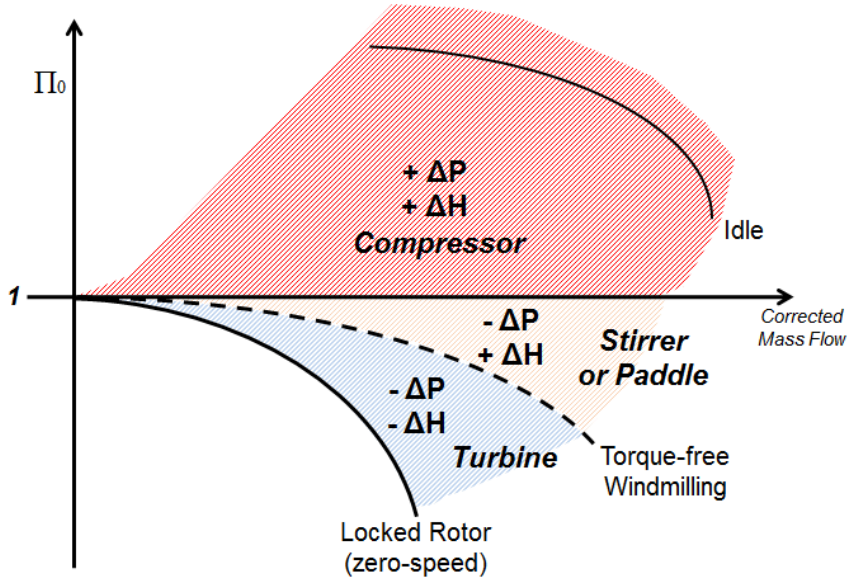

Figure 1 Sub-idle compressor map.

The sub-idle portion of a map can be divided into three distinct regions depending on the sign of the work and total pressure changes, as in Figure 1. While any point with a pressure ratio above unity is considered inside the compressor operation region, the regions with a total pressure loss can be divided into stirrer and turbine modes depending on the sign of the work input. In the stirrer mode, there is a work addition to the flow along with a pressure loss, while work extraction and pressure loss define the turbine mode. A key element of the map is the boundary between these last two regions, which corresponds to the torque-free windmilling characteristic [3]. At this torque-free windmilling characteristic, there is no net torque on the shaft and no net work done on the gas. In the absence of loads and frictional losses, the torque-free windmilling line could be reached by a compressor simply due to the incoming flow. In a real-life application, frictional losses result in steady state windmilling operation occurring slightly below the torque-free windmilling line, marginally in the turbine region [4]. At the lower extreme of the map, the locked rotor line corresponds to zero speed operation, where flow simply passes through the compressor, incurring a pressure loss and imparting torque on the shaft. Due to the net enthalpy change (ΔH) becoming zero at the windmilling line, performance parameters containing an enthalpy term in the denominator are not continuously defined throughout the sub-idle region. For this reason, the corrected torque parameter (τ_P) is used alongside the pressure ratio and corrected mass-flow to describe compressor performance in the sub-idle region [5]. This parameter is defined as the shaft torque divided by inlet total pressure.

In order to accurately predict whole-engine performance using a zero-dimensional performance solver, maps are required for the different engine components. As data in these regions is scarce and not generally obtained from rig tests, a way to generate these maps needs to be devised. Several techniques have come about for the generation of sub-idle compressor maps using a variety of graphical [6], and analytical methods [7-8]. These are generally low-fidelity approximations that limit the accuracy of the generated performance data. A review of these methods can be found in Jones et al. [9]. Previous work at Cranfield University has looked at enhancing map generation by including interpolation from limited sub-idle data, such as locked rotor and windmilling characteristics [10-11]. While these last methods have shown to result in viable maps, they highlight the need to accurately calculate the locked rotor and, especially, windmilling characteristics to further improve the reliability of the maps generated.

The numerical scheme presented in Righi et al. [12] has shown the capability to model compressor operation at extreme off-design cases, and as such is a strong candidate for application to the sub-idle case. This paper concerns itself with the adaptation of the through-flow code presented in that work to sub-idle modelling along with validation against experimental data. The significance of these simulation results is that they may be used as inputs to the map generation method presented in Ferrer-Vidal et al. [11], yielding compressor maps of improved accuracy.

2.0 EXPERIMENTAL METHOD

An experimental sub-idle rig is required to generate the sub-idle data needed for validation. The data is gathered in the form of locked rotor and windmilling characteristics, which do not require the compressor to be powered. A Rolls-Royce Allison Model 250 (M250) C20b axial compressor assembly is used. The rig includes pressure rakes upstream and downstream of the compressor, an optical shaft speed sensor, and a downstream settling duct and venturi flow meter. The compressor is unpowered, with an extraction fan and butterfly valve used to set the mass-flow. The shaft is locked to obtain the locked rotor characteristic and freed to obtain the windmilling line. The rig arrangement is shown in Figure 2.

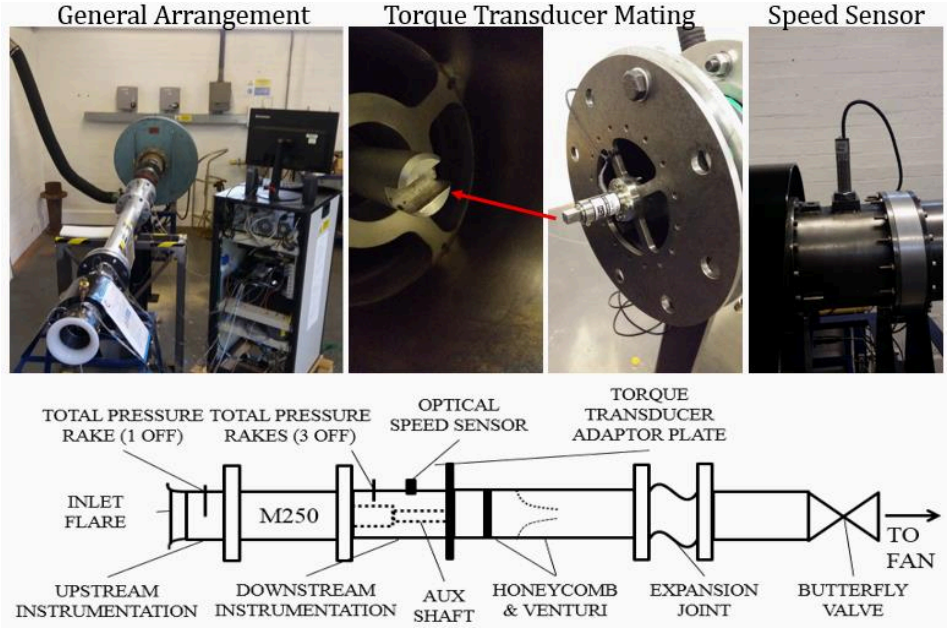

Figure 2 Sub-idle rig arrangement schematic and pictures from the original experiment.

A torque transducer is used to lock the compressor shaft for locked rotor studies and measure the torque. The transducer is placed on an adaptor plate while a groove in a compressor shaft extension allows the coupling of the transducer. The shaft speed is measured via an optical speed sensor which reads off a sticker placed on the shaft extension. A more detailed description of the rig may be found in Ferrer-Vidal et al. [11].

3.0 LOW-ORDER MODEL

The low-order models presented here are a direct application of the through-flow code originally described by Righi et al. [12] which has been modified to introduce sub-idle modelling. An overview of the through-flow code is first given, followed by a description of the three different methods used to model the performance of blade rows in sub-idle conditions.

The code was originally created to handle compressor surge transients, where a 3D formulation is required for the proper simulation of stall cells. The flow is considered to

be axisymmetric for the purpose of obtaining sub-idle characteristics, allowing a 2D formulation. The flow equations are solved transiently on a relatively coarse grid, as required to maintain acceptable computational performance. A structured mesh is generated based only on the annulus geometry, requiring the number of elements in each geometric direction as an input, but with no need for detailed mesh generation.

The equations solved are the unsteady, compressible, cylindrical Euler equations, and may be written in matrix form as:

$$\frac{\partial}{\partial t}\begin{bmatrix}\rho\\ \rho u_r\\ \rho u_\theta\\ \rho u_x\\ \rho E_0\end{bmatrix} = -\frac{1}{r}\frac{\partial}{\partial r}\begin{bmatrix}\rho r u_r\\ \rho r u_r^2\\ \rho r u_\theta u_r\\ \rho r u_x u_r\\ \rho r H_0 u_r\end{bmatrix} - \frac{1}{r}\frac{\partial}{\partial \theta}\begin{bmatrix}\rho u_\theta\\ \rho u_r u_\theta\\ \rho u_\theta^2 + P\\ \rho u_x u_\theta\\ \rho H_0 u_\theta\end{bmatrix} - \frac{\partial}{\partial x}\begin{bmatrix}\rho u_x\\ \rho u_r u_x\\ \rho u_\theta u_x\\ \rho u_x^2 + P\\ \rho H_0 u_x\end{bmatrix} + \begin{bmatrix}0\\ \frac{\rho u_\theta^2}{r} + \frac{\partial P}{\partial r} + f_r\\ -\frac{\rho u_\theta u_r}{r} + f_\theta\\ f_x\\ W_{EX}\end{bmatrix} \quad (1)$$

where f_r, f_θ, f_x, W_{EX} are source terms introduced by the body-force method.

The Godunov scheme is used for the solution of Equation 1. This is a first-order accurate, monotone, finite volume scheme where inter-volume fluxes are calculated based on the solution of the local Riemann problem. It is total-variation diminishing (TVD) preventing unphysical solutions from arising [13] but, as a first order method, it introduces substantial numerical diffusivity. Because of their diffusivity, first order schemes are not generally considered accurate for traditional CFD [14]; however in the current application, in which highly separated flows are modelled using Euler equations, the numerical diffusion is considered advantageous as it helps stabilize the simulation.

To simulate the presence of the blades, the body-force method is used. There is no resolution of the flow-field inside the channels; instead, the flow inside each grid element is considered as a pitch-wise average of the flow inside one or more channels. The body forces introduce the effect of the blade as a turning and a total pressure loss. This requires the knowledge of the performance of the blade, in the form of a deviation δ and a total pressure loss, expressed as a pressure loss coefficientω. The formulations used here to calculate the forces are derived from what is proposed in Longley [15] and Brand [16]. The forces are decomposed and applied onto the grid in the radial, circumferential, and axial directions, represented by f_r, f_θ, f_x in the source term of Equation 1. A work exchange term (W_{EX}) is also included, which accounts for the rotor work input to the flow as a result of the flow turning. A detailed explanation of this methodology is found in Righi et al. [12].

Non-reflecting boundary conditions are applied at the inlet and outlet of the model [17]. A total pressure and temperature inlet boundary condition is used along with a static pressure outlet. To generate characteristics, the outlet static pressure is lowered incrementally to simulate throttling. For the locked rotor case, the model RPM is set to zero. For the windmilling case, the torque is integrated over all the elements inside of the rotors and a simple balance equation is used to alter the rotational speed as shown in Equation 2. The rotational speed changes until the torque matches the target value τ_{target}; this is set to zero for zero-torque windmilling case but it can also be used to introduce friction or an external force on the shaft (e.g. cranking). As the code uses a transient formulation, a shaft inertia I must be input by the user. Since in this study only the steady-state solution is of interest, the inertia is set to a very low value to accelerate convergence.

$$\Omega^{t+1} = \Omega^t + \frac{\sum \tau + \tau_{target}}{I} \cdot dt \quad (2)$$

As mentioned, the through-flow code requires knowledge of blade performance in the form of total pressure loss and deviation angle. For the sub-idle case, three different blade performance models are implemented independently and their results compared. These models and their relative merits are described below.

3.1 Separated passage flow model

The through-flow code employs a passage blockage method originally proposed by Longley [15] to model the performance of blade rows in reverse flow conditions. This methodology has been described in Righi et al. [12] as part of the reverse flow treatment used in modelling compressor stall transients. In this paper, the adaptation of this approach for use in sub-idle modelling due to the similarities between the flow regimes is proposed.

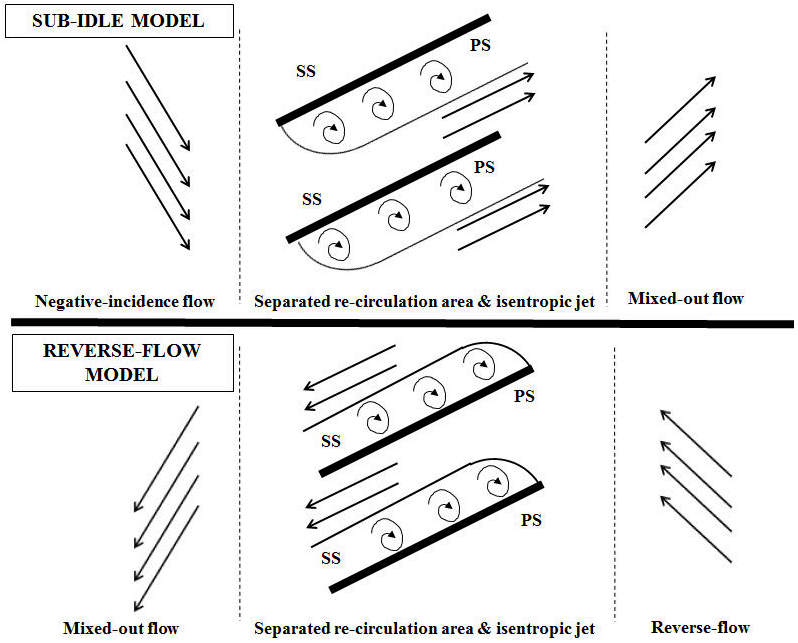

Figure 3 Sub-idle flow model (top) and reverse flow model as presented in [15] (bottom).

During sub-idle operation, low blade speed combined with comparatively large mass-flow results in operation at high flow coefficient and highly negative blade incidence angles. Due to these highly negative incidences, the flow separates from the pressure side (PS) of the blade, while remaining well attached to the suction side (SS) [18]. The situation is very similar to the reverse flow model developed by Longley [15], where the flow is considered to be split into an isentropic jet closely attached to the blade pressure side along with a separated low-momentum region on the suction side. For this sub-idle model, we instead consider the isentropic jet to remain attached to the suction side, with the low-momentum separated region on the pressure side a result of the negative incidence flow. Figure 3 shows the similarities between the original reverse flow model from Longley [15] and its application to sub-idle within this work.

The isentropic jet is considered to exit the passage parallel to the blade chord, with a flow angle equal to the blade stagger angle. The recirculation region is considered to be of negligible mass-flow. A b parameter is defined analogously to that presented by Longley as the ratio between the real axial momentum of the separated flow and the axial momentum of a pitch-wise averaged flow. This parameter thus characterizes the flow non-uniformity arising as a result of the pressure side recirculation region present at sub-idle. The b parameter is calculated from the inlet flow angle and blade stagger as shown in Equation 3.

$$b = 1 + \left|\frac{\sin(\alpha_{IN} - \gamma)}{\cos(\alpha_{IN})}\right| \qquad (3)$$

As opposed to the method proposed by Longley, the model presented here does not account for the transport of this b parameter. The mixing of non-uniform flow is thus modelled as occurring instantaneously, resulting in a deviation angle of the mixed-out flow solution. The point at which maximum blockage is reached is set at a quarter of the chord and from this point the profile of b in the passage is modelled based on a prescribed mixing ratio. We can then estimate the value of b at the trailing edge, from

which the mixed-out flow angle can be calculated. As a result of the mixing, the deviation angle also becomes a function of the blade solidity in addition to the stagger angle. This mixed-out deviation angle is then imposed on the flow via the body-force method.

Skin friction losses are not considered, as separation is deemed to be the dominant loss mechanism. Losses due to separation are introduced by modifying the direction in which body forces are imposed. This foregoes the need for loss correlations. This pressure loss treatment does not need the flow to enter at the leading edge and exit at the trailing edge, allowing for re-circulating and reversed flow conditions to be treated. On the other hand the deviation model used needs the blade passage inlet and outlet to be uniquely defined, not being able to handle recirculation. In such a case, the deviation is set to 0 degrees.

3.2 Sub-idle correlations

The classical approach to modelling blade row performance is through the use of empirical correlations. As no correlations spanning the negative incidence range typical of sub-idle operation are available in the literature, a set of (as yet unpublished) correlations tailored to negative incidences has been developed by Cranfield University which predict both deviation and pressure loss for a range of inlet conditions. The correlations are derived from a campaign of 2D CFD simulations of a typical modern HPC rotor blade row at mid-span. These simulations encompass the full negative incidence range down to $i = -90\ deg$, including cases with pressure side separation as shown in Figure 3. The campaign was performed using steady state RANS simulations to reduce the computational cost. In a separate study, the locked rotor characteristic of a 3D single-stage model was generated using RANS simulations and time-accurate URANS SAS (Unsteady Reynolds Averaged Navier-Stokes Scale Adaptive Simulation) and SBES (Stress Blended Eddy Simulation, a hybrid RANS-LES formulation). Although the sub-idle condition is substantially unsteady, the time-average of the results from the unsteady simulations closely match the results from the RANS formulation, suggesting that the latter are appropriate for the creation of correlations and characteristics [19]. The blade row is simulated for a range of Mach numbers, inlet angles and Reynolds numbers; the blades are also rotated and translated rigidly to test different solidities and stagger angles. The domain extends several chord lengths after the blade row to ensure the wakes from the separated passages are fully mixed; the deviation and pressure loss are then calculated considering the fully mixed out flow at domain outlet.

The database created from the CFD results is used to train a neural network, creating an algorithm to predict the performance based on blade geometry and inlet conditions:

$$(\omega, \delta) = f(\gamma, \sigma, i, M_{IN}, Re_{IN}) \qquad (4)$$

In this method the body forces used are always aligned with the flow and do not introduce any additional pressure loss, but only that predicted by the correlation. Unlike the separated passage flow model, these correlations cannot work when recirculation is present in the blade passage. In this case, the deviation is set to 0 degrees and no pressure loss occurs.

3.3 Hybrid method

The flexibility granted by the separated passage flow model during transients and in case of recirculation is very useful, especially in cases where we expect the flow to develop recirculation or strong radial flow. However, the deviation calculated with the analytical model in Figure 3 is based on an incompressible flow, does not include the inlet Reynolds number, and is based on the assumption of the blade behaving like a flat plate.

The simplified deviation treatment is arguably the crudest assumption in the separated a passage model. To possibly improve on this, a hybrid approach is proposed where the deviation obtained from the sub-idle correlations is used to determine the flow turning imposed by the body forces in the separated passage flow model. The pressure loss instead is introduced by stream-wise components of the turning forces as in the

separated passage flow model. This hybrid method is implemented in the through-flow code and the results are compared to those obtained with the 2 models described above.

4.0 RESULTS AND DISCUSSION

The low-order numerical models described are used to obtain the locked rotor characteristic and windmilling lines for an Allison M250 axial compressor rig, which has been tested under sub-idle conditions at Cranfield University. The characteristics obtained are compared to experimental data reported by Ferrer-Vidal et al. [11] and 3D RANS CFD simulations of the same compressor.

With the through-flow code, each characteristic is created by running only a few simulations in which the boundary conditions are changed in steps and leaving enough time between steps so that the flow can reach steady conditions. The flow at each steady state is then post-processed to create the points which form the characteristic. The overall computational time depends on the number of points required, but it varies between 20 and 40 minutes per characteristic using a single quad-core desktop workstation. For comparison, the time required to obtain a single operating point with the 3D CFD model is about 24 hours using 64 CPUs on a high performance computing facility.

4.1 Grid convergence study for the through-flow code

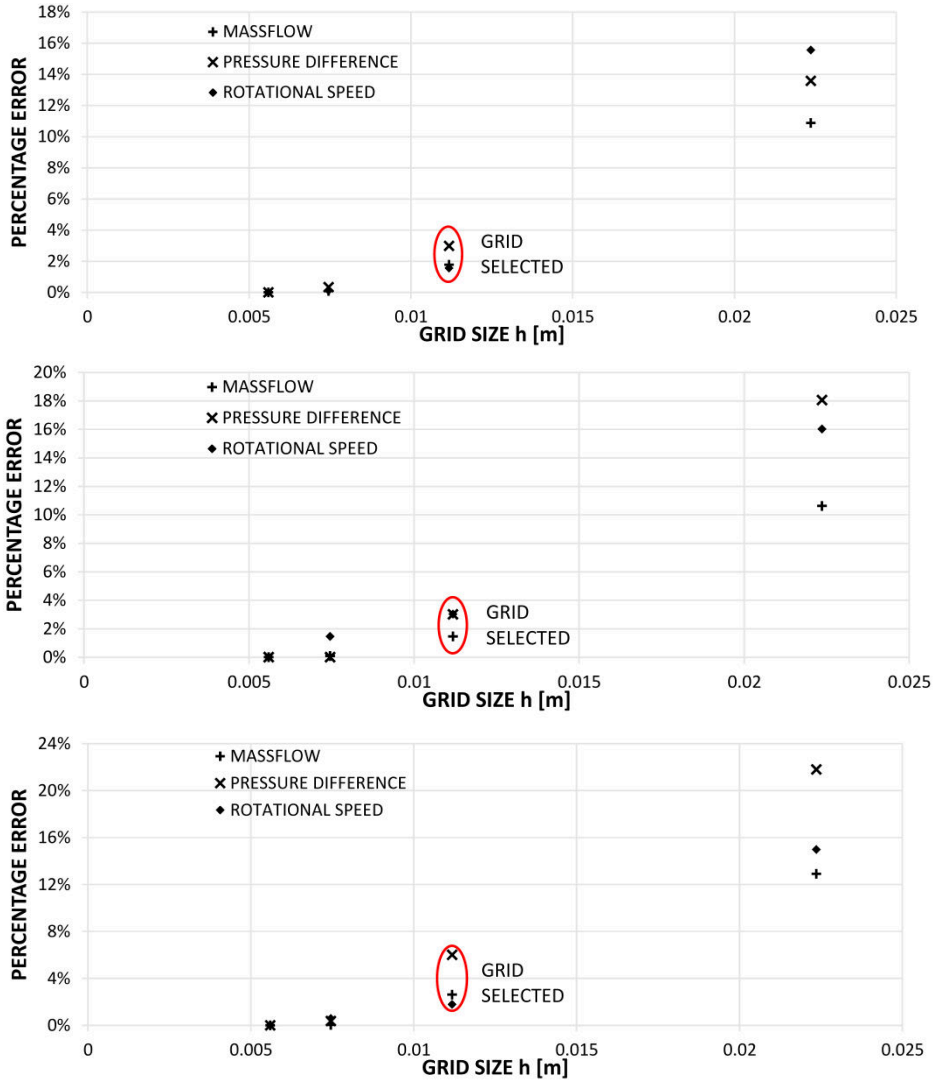

Figure 4 Convergence study for the low-order models; separated passage flow model (top), sub-idle correlation (middle), hybrid method (bottom).

The inlet and outlet domains are both extended axially by a length equivalent to one mean radius. The grid used in all the low-order simulations has 800 axial and 10 radial elements. A convergence study was run on a steady windmilling case for all 3 low-order models. The convergence study is shown in Figure 4; the mass-flow, pressure difference across the compressor and rotational speed are shown as percentage discrepancy for different grid size. The percentage discrepancy is defined as:

$$(X - X_{FINE})/X_{FINE} \qquad (5)$$

where X is the variable considered. The grid size h is calculated as defined by Celik [20]:

$$h = \left[\frac{1}{N}\sum_{i=1}^{N}(\Delta A_i)\right]^{1/2} \qquad (6)$$

where N is the number of elements, and ΔA_i is the area of the i^{TH} element. The grids considered for all models are 400 axial elements by 5 radial elements, 800 by 10, 1200 by 15, and 1600 by 20. All the models show convergence, with the selected grid having less than 6% percentage discrepancy from the finest on all the variables.

4.2 Locked rotor simulation

The pressure and torque characteristic for the locked rotor case are reported in Figure 5 and Figure 6. The torque is presented using the corrected torque parameter τ_P (torque over inlet total pressure). In both cases the sub-idle correlations have the best matching with the experimental results while the separated passage flow model has the worst. All low-order models under-estimate the mass-flow in the range considered.

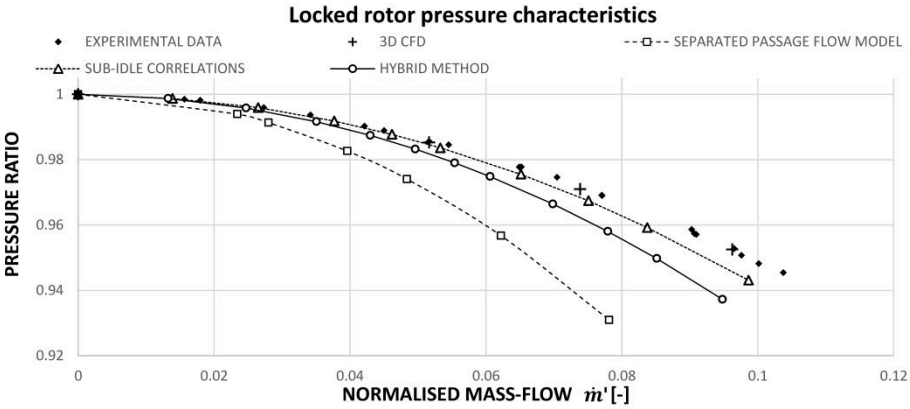

Figure 5 Comparison of locked rotor pressure characteristics from experimental data, CFD and low-order models.

The experimental data available does not extend until the choking conditions. The choking conditions were instead investigated using 3D CFD and the sub-idle correlations model, as these show the closest matching. The results are reported in Figure 7. An exit-corrected mass-flow rate boundary condition is applied on the CFD modelling, allowing the entire characteristic to be investigated. This allows the exit-corrected mass-flow to be increased progressively until no further increase in actual mass-flow occurs in the model, representative of choking conditions. The low-order model is run reducing the pressure at domain outlet until the flow reaches choking condition and the mass-flow stops increasing. The two characteristics diverge at higher mass-flows, and the discrepancy from the CFD results is ~10% in pressure ratio close to choking conditions.

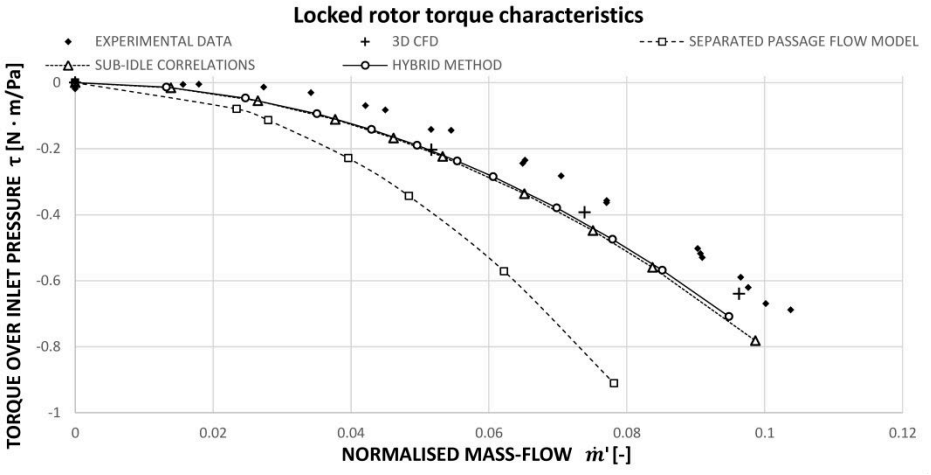

Figure 6 Comparison of locked rotor torque characteristics from experimental data, CFD and low-order models.

The low-order models employ a body-force method which does not introduce the effect of blade thickness on the passage area and do not force the flow to follow exactly the blade local camber-line direction. As a result, the choking conditions are expected to occur at a higher mass-flow than in reality (or using 3D CFD). However, close to choking conditions the sub-idle correlations introduce a sharp increase in pressure loss coefficient, causing the pressure characteristic to become steeper. As a result the mass-flow at which choking conditions occur is close to the value obtained through CFD.

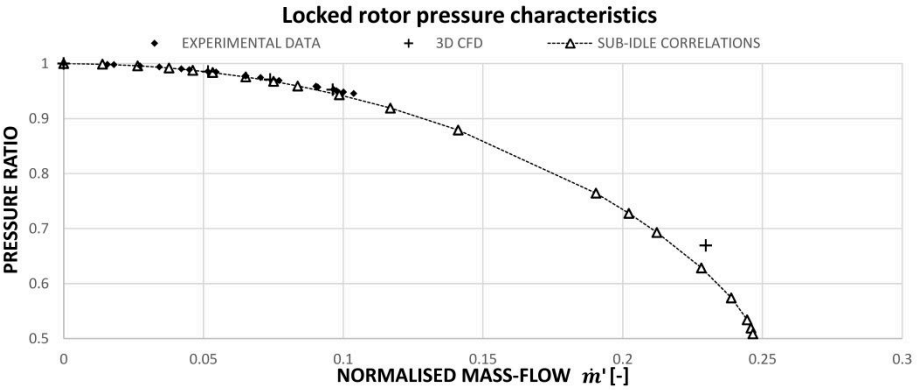

Figure 7 Comparison of locked rotor pressure characteristic close to choking conditions.

4.3 Windmilling simulations

The experimental rig was run in windmilling conditions to obtain the pressure characteristic and the windmilling signature line. However, in a real experiment a small resistant torque due to friction in the bearings is always present. As a result, the experimentally measured signature line does not pass through the origin of the chart. In order to account for this difference, a frictional torque is added to the model employing the sub-idle correlation. By modelling a single experimental point ($\dot{m}' = 0.1173$) and matching pressure ratio and rotational speed, the mass-flow is found to match closely the experimental value (modelled $\dot{m}' = 0.1185$) and a mismatch in torque is found ($\tau_P = 0.0576\ N \cdot m/Pa$). This torque mismatch is due to both friction present in the real compressor and inaccuracy of the model. This torque is assumed to be all due to friction and implemented in the model as a constant resistant torque. The windmilling characteristic with friction is then created and it shows alignment not only to the point used to estimate the torque itself, but to the full range of experimental data. The characteristics created with sub-idle correlations, with and without friction, are presented in Figure 8 and Figure 9, and compared to experimental data and 3D CFD (without friction). The rotational speed Ω' is normalised using the design value of speed.

In both figures it can be observed that at high mass-flow the characteristic and windmilling signature line with and without friction become closer asymptotically. This occurs because, as the mass-flow increases, the resistant torque becomes less important with respect to the torque exchanged between the front and the rear stages of the compressor. At high mass-flows the experimental signature line aligns to the friction-less model line, which passes through the origin of the chart. At low mass-flow instead, it diverges and has lower rotational speed; the same behaviour is reproduced by the low-order model with friction.

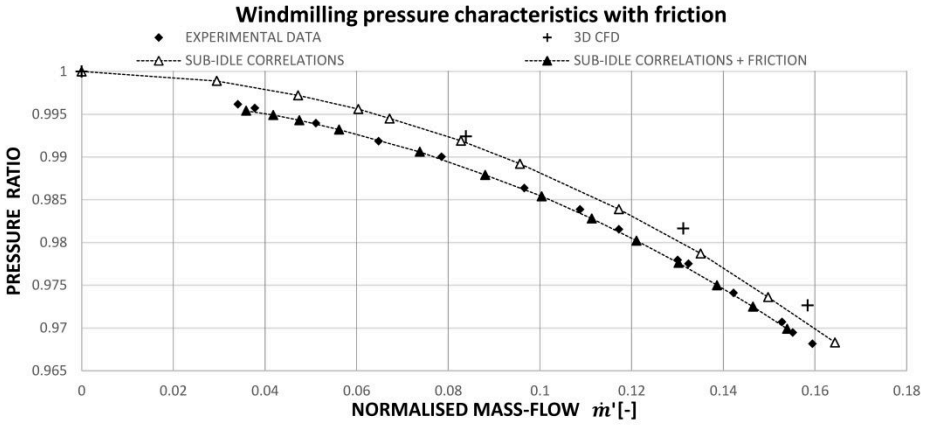

Figure 8 Comparison of windmilling pressure characteristics from experimental data, CFD (without friction) and a low-order model with and without friction.

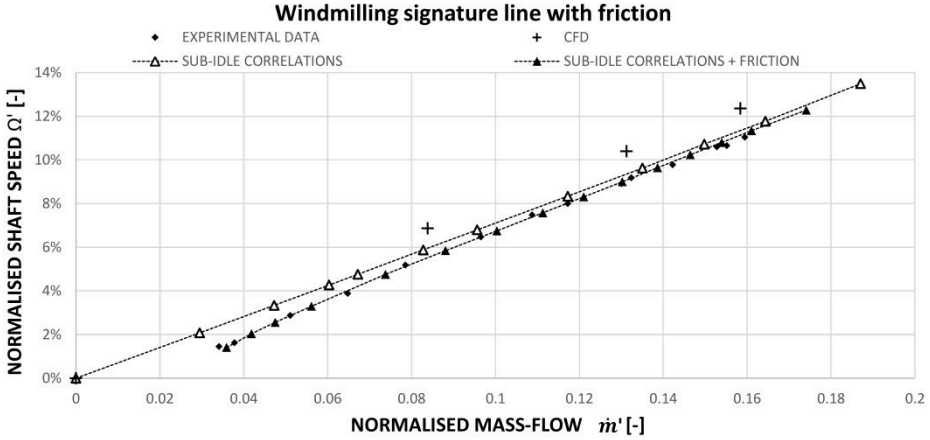

Figure 9 Comparison of windmilling signature line from experimental data, CFD (without friction) and low-order model with and without friction.

The results of zero-torque windmilling simulations (no friction) obtained with the low-order model are reported in figures Figure 10 - Figure 11 and compared to the 3D CFD results and experimental data. The sub-idle correlations have the best matching with the CFD results and with experimental data at high mass-flow. The value of the signature line slope predicted by the low-order models are reported in Table 1 and compared with the experimental data. The experimental signature line slope is obtained by fitting the data linearly; to reduce the effect of the friction on the line slope only the data with $\dot{m}' > 0.09$ are considered.

Table 1
Comparison of experimental and modelled windmilling signature line slope

	Windmilling signature line slope	Discrepancy from experimental data
Experimental data	0.715	/
CFD	0.738	3.1%
Separated passage flow model	0.924	29.2%
Sub-idle correlations	0.724	1.3%
Hybrid method	0.722	1.0%

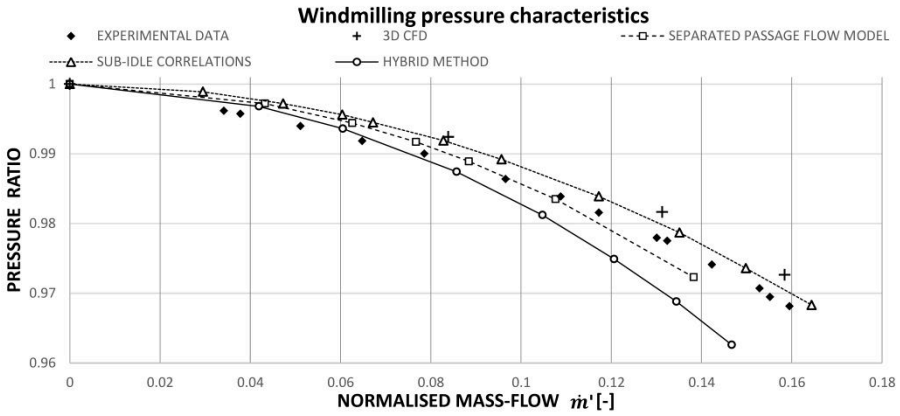

Figure 10 Comparison of zero-torque windmilling pressure characteristics from experimental data, CFD and low-order model.

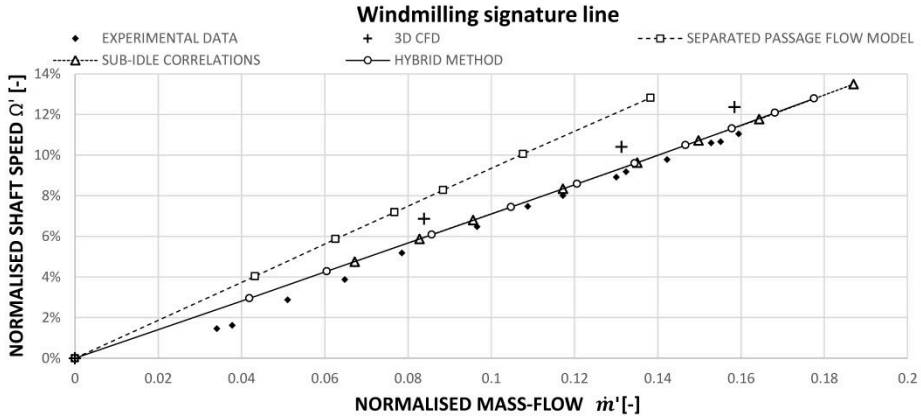

Figure 11 Comparison of windmilling signature line from experimental data, CFD and low-order models.

The distribution of the torque in the different blade rows during windmilling is presented in Figure 12, with the results obtained from the sub-idle correlations low-order model and 3D CFD. The simulations are run in zero torque conditions with the same mass-flows: case 1 $\dot{m}' = 0.086$, case 2 $\dot{m}' = 0.162$. The torque presented has been normalised using the value at the first rotor, the normalised torque of the n blade row is then: $\tau'_n = \tau_{P\,n}/\tau_{P\,1}$. It can be observed that the distribution predicted by each model remains largely constant at different mass-flows. The constant axial distribution of normalised torque with different mass-flows is another indication that the windmill condition can be characterized as a non-dimensional operating point [11-21-22]. Such a

point can be described by a single flow and work coefficient pair for the entire machine; or indeed for each individual stage.

Both models predict that the first 4 rows have a positive torque, introducing energy in the flow, and the last 2 have negative torque and extract energy from the flow. As the distribution does not change, this structure remains constant for the mass-flow range considered.

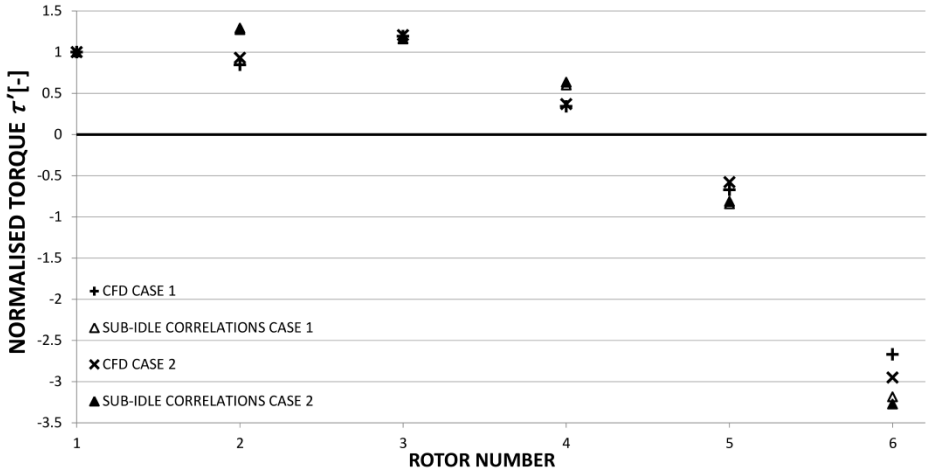

Figure 12 Torque distribution between the rotors at zero-torque windmilling conditions. Case 1 $\dot{m}' = 0.086$, case 2 $\dot{m}' = 0.162$.

Overall the low-order model using the sub-idle correlations has the best match with experimental data and 3D CFD in all cases presented.

Despite having different pressure characteristic, the low-order models using sub-idle correlations and hybrid method have very similar results for torque characteristic (at locked rotor conditions) and windmilling signature. This suggests that these two characteristics, which link mass-flow and torque, are mainly driven by deviation (the two models share the same method to estimate it), and are not strongly influenced by the pressure loss.

5.0 CONCLUSIONS

In this paper different low-order methods to model the performance of blade rows in sub-idle conditions have been presented and used in the generation of locked rotor and windmilling characteristics with a through-flow code. The cases studied include pressure and torque characteristics in the locked rotor case, and the pressure characteristic and signature line in zero-torque windmilling conditions. The characteristics generated are compared to experimental data and 3D RANS CFD simulation. The low-order model employing the correlations for sub-idle conditions developed in Cranfield University reproduced every characteristic with close matching to experimental data and CFD. The introduction of an input torque in the code allows the modelling of friction or external cranking, as during engine starting. Using a resistant torque, the effect of friction observed in the experimental windmilling tests has been reproduced and closely matched. The distribution of work exchange along blade rows during wind-milling has also been investigated and successfully matched with results from CFD.

The code presented requires as input only the basic geometry of the blades and the annulus and can therefore be used to evaluate the compressor sub-idle performance at an early design stage. This can be used to simulate the cranking and starting of a gas turbine for both propulsion and power generation applications. Furthermore the sub-idle characteristics can be used to simulate the condition of altitude re-light, which is an important requirement for aero-engines.

The through-flow code represents a fast alternative to 3D CFD, allowing the creation of a full characteristic in less than an hour. When coupled with a map generation technique taking locked rotor and windmilling characteristics as inputs [11], such a model has the capability to produce compressor sub-idle maps in a time and accuracy unrivalled by existing approaches.

ACKNOWLEDGEMENTS

This project has received funding from the Clean Sky 2 Joint Undertaking under the European Union's Horizon 2020 research and innovation programme under grant agreement No 785349. Data subject to third party restrictions.

REFERENCES

[1] EASA, "Certification Memorandum: Turbine Engine Relighting in Flight," Pub. L. No. CS-E 910, 2015.

[2] P K ZACHOS, "Modelling and analysis of turbofan engines under windmilling conditions," *Journal of Propulsion and Power*, vol. 29, no 4, pp. 882- 890, 2013.

[3] Z Q SHOU, "Calculation of windmilling characteristics of turbojet engines," *Journal of Engineering for Power,* vol. 103, no 1, pp. 1-12, 1981.

[4] P P WALSH, P P FLETCHER,"Gas turbine performance," John Wiley & Sons, 2004.

[5] C RIEGLER, M BAUER, J KURZKE, "Some aspects of modelling compressor behavior in gas turbine performance calculations," A*SME Turbo Expo 2000: Power for Land, Sea, and Air*, pp. 1- 8, 2000.

[6] J KURZKE, "How to get component maps for aircraft gas turbine performance calculations," *ASME 1996 International Gas Turbine and Aeroengine Congress and Exhibition,* pp. 1- 8, 1996.

[7] R K AGRAWAL, M YUNIS, "A generalized mathematical model to estimate gas turbine starting characteristics," *ASME 1981 International Gas Turbine Conference and Products Show*, pp. 1-8, 1981.

[8] S R GAUDET, J E D GAUTHIER, "A simple sub-idle component map extrapolation method," *ASME Turbo Expo 2007: Power for Land, Sea, and Air*, pp. 29-37, 2007.

[9] G JONES, P PILIDIS, B CURNOCK, "Compressor characteristics in gas turbine performance modelling," *ASME Turbo Expo 2001: Power for Land, Sea, and Air*, pp. 1-7, 2001.

[10] P K ZACHOS, C RUELKE, V PACHIDIS, R SINGH, "Compressor blade modelling under highly negative incidence," *ASME 2011 Turbo Expo: Turbine Technical Conference and Exposition*, pp. 431- 441, 2011.

[11] L E FERRER-VIDAL, V PACHIDIS, R J TUNSTALL, "An enhanced compressor sub-idle map generation method," *Proceedings of GPPS Forum 2018, 10-12 January 2018, Zurich, Switzerland,* 2018.

[12] M RIGHI V PACHIDIS L KÖNÖZSY L PAWSEY, "Three-dimensional through-flow modelling of axial flow compressor rotating stall and surge," *Aerospace Science and Technology*, vol. 78, pp. 271-279, 2018.

[13] E TORO, "Riemann solvers and numerical methods for fluid dynamics: a practical introduction," Springer Science & Business Media, 2007.

[14] C HIRSCH, "Numerical Computation of Internal and External Flows, Vol.1: Fundamentals of Computational Fluid Dynamics," Elsevier, 2nd edition, 2007.

[15] J P LONGLEY, "Calculating stall and surge transients," *ASME Turbo Expo 2007: Power for Land, Sea, and Air*, pp. 125-136, 2007.

[16] M L BRAND, "An improved blade passage model for estimating off-design axial compressor performance," PhD thesis, Massachusetts Institute of Technology, 2013.

[17] T J POINSOT, S K KELE, "Boundary conditions for direct simulations of compressible viscous flows," *Journal of computational physics*, vol. 101, no 1, pp.

104-129, 1992.

[18] E ILLANA, N GRECH, P K ZACHOS, V PACHIDIS, "Axial compressor aerodynamics under sub-idle conditions," *ASME Turbo Expo 2013: Turbine Technical Conference and Exposition*, pp. 1-11, 2013.

[19] A I PEREZ, "Scale-resolving simulations of compressor blading at negative incidences," MSc thesis, Cranfield University, 2018.

[20] I B CELIK, "Procedure for estimation and reporting of discretization error in cfd applications," *Journal of Fluids Engineering*, vol. 130, no 7, pp. 1-4, 2008.

[21] E J GUNN, C A HALL, "Loss and deviation in windmilling fans," *Journal of Turbomachinery*, vol. 138, no 10, pp. 1-9, 2016.

[22] N BINDER, S COURTY-ADREN, S DUPLAA, G DUFOUR, X CARBONNEAU, "Theoretical analysis of the aerodynamics of low-speed fans in free and load-controlled windmilling operation," *Journal of Turbomachinery*, vol. 137, no 10, pp. 1-12, 2015.

2019-09-27

Low-order models for the calculation of compressor sub-idle characteristics

Righi, Mauro

ISABE

Righi M, Ferrer-Vidal LE, Allegretti A, Pachidis P. (2019) Low-order models for the calculation of compressor sub-idle characteristics. In: ISABE 2019: 24th Conference of the International Society of Air Breathing Engines, 22-27 September 2019, Canberra, Australia. Paper number 24197 https://isabe.org/